Available online at www.sciencedirect.com
SCIENCE DIRECT®
International Journal of Heat and Mass Transfer 47 (2004) 2109–2122
International Journal of HEAT and MASS TRANSFER
www.elsevier.com/locate/ijhmt

Large eddy simulation of a thermally stratified turbulent channel flow with temperature oscillation on the wall

Yu-Hong Dong, Xi-Yun Lu *

Department of Modern Mechanics, University of Science and Technology of China, Hefei, Anhui 230026, China

Received 24 July 2003; received in revised form 6 December 2003

Abstract

Thermally stratified turbulent channel flow with temperature oscillation on the bottom wall of the channel is investigated by use of large eddy simulation (LES) approach coupled with dynamic subgrid-scale (SGS) models. The objective of this study is to deal with the influence of the temperature oscillation on characteristics of thermally stratified turbulent flow and to examine the effectiveness of the LES technique on predicting unsteady turbulent flow driven by time-varying buoyancy force. To validate the present calculation, thermally stratified turbulent channel flow is computed and compared with available data obtained by direct numerical simulation (DNS), which confirm that the present approach can be used to study stably and unstably stratified turbulent flow satisfactorily. Further, to elucidate the effect of the temperature oscillation on turbulent flow with different Richardson numbers and oscillation periods, some statistical quantities including the phase-averaged resolved velocities, temperature and their fluctuations, turbulent heat fluxes, and turbulence structures based on instantaneous velocity and temperature fluctuations are analyzed.

Keywords: Large eddy simulation (LES); Turbulent channel flow; Thermally stratified turbulence; Subgrid scale (SGS) model; Heat transfer; Temperature oscillation

1. Introduction

Thermally stratified shear turbulence is a kind of complex flow driven by both shear and buoyancy forces. Inherent unsteadiness of driving condition (e.g., time-varying buoyancy force) occurs extensively in natural phenomena and engineering applications and characterizes a variety of time-dependent thermal turbulent flows. For example, in the oceans, where the thermocline plays an important role, the value of the Brunt–Väisälä frequency changes from 1 up to 10 cycles for hour [1]; the Richardson number thus varies in time rather than in constant value. It indicates that thermal flows associated unsteady heating conditions are general. Meanwhile, turbulent flow coupled with heat transfer is important in the fundamental research of turbulence. To the best of our knowledge, however, thermally stratified turbulent channel flow with temperature oscillation on the bottom wall of the channel, where statistically unsteady turbulent flow is driven by time-varying buoyancy force, can be employed as a typical case for unsteady thermal turbulent flow and has never been examined. In the following, the relevant work on thermally stratified shear turbulent flows and statistically unsteady turbulent flows driven by time-varying forces is briefly reviewed.

The first study of stratified homogeneous shear flows was taken by Rohr et al. [2], who showed that, at a gradient Richardson number of about 0.25, the turbulence neither grows nor decays. At lower Richardson numbers, the turbulent kinetic energy grows; at higher ones, the turbulence decays. Direct numerical simulation (DNS) of stably stratified sheared homogeneous

* Corresponding author. Tel.: +86-551-3603223; fax: +86-551-3606459.
E-mail address: xlu@ustc.edu.cn (X.-Y. Lu).

0017-9310/$ - see front matter © 2004 Elsevier Ltd. All rights reserved.
doi:10.1016/j.ijheatmasstransfer.2003.12.011

Nomenclature

E_k	volume-integrated turbulent kinetic energy
E_{kP}	phase-average of the volume-integrated turbulent kinetic energy
f	frequency of temperature oscillation
$F(v')$	flatness factor of the wall-normal velocity fluctuation
$F(w')$	flatness factor of the spanwise velocity fluctuation
g	gravitational acceleration
$S(v')$	skewness factor of the wall-normal velocity fluctuation
$S(w')$	skewness factor of the spanwise velocity fluctuation
t_P	period of temperature oscillation
$\overline{T}$	resolved temperature
T'	resolved temperature fluctuation
T_B	temperature on the bottom wall of the channel
T_U	temperature on the upper wall of the channel
C	SGS model coefficient
$\bar{p}$	resolved modified pressure
Pr	Prandtl number
Pr_T	turbulent Prandtl number
q_i	SGS turbulent heat flux
Re_τ	Reynolds number based on the friction velocity
Ri_b	Richardson number based on the bulk velocity
Ri_τ	Richardson number based on the friction velocity
$\overline{S}_{ij}$	resolved strain rate tensor
t	time
u	resolved streamwise velocity
u'	resolved streamwise velocity fluctuation
$\bar{u}_i$	resolved velocity
u'_i	resolved velocity fluctuation
u_τ	friction velocity of unstratified turbulent channel flow
v	resolved wall-normal velocity
v'	resolved wall-normal velocity fluctuation
w	resolved spanwise velocity
w'	resolved spanwise velocity fluctuation
x_i	Cartesian coordinate axes
y	wall-normal coordinate
y^+	wall-normal coordinate normalized by the friction velocity
β	thermal expansion coefficient
δ	half-width of the channel
$\overline{\Delta}$	size of grid filter
$\widehat{\overline{\Delta}}$	size of test filter
τ_{ij}	SGS turbulent stress tensor
ν	molecular kinematic viscosity
κ	thermal diffusivity
$\langle\ \rangle$	phase-average at the same phase and space-average over the plane parallel to the wall
$\langle\ \rangle_S$	space-average over the plane parallel to the wall
$\langle\ \rangle_T$	time-average in the whole time region and space-average over the plane parallel to the wall

Subscript

rms	root mean square

Superscript

+	normalized quantity by wall parameters

turbulence was performed by Gerz et al. [3] and demonstrated the presence of persistent counter-gradient fluxes at small scales under strong stratification. For stratified wall-bounded flows, the qualitative difference between the inner and outer layers of turbulent wall-bounded flows along with the spatial inhomogeneity of the flow introduces different Richardson numbers as relevant parameters. Typically, Iida and coworkers [4,5] performed the DNS to study unstably and stably stratified turbulent channel flows. Internal gravity wave for stably stratified turbulent channel flow was found to be built up in the core region, where the turbulent heat flux is suppressed drastically and the steep mean velocity and temperature gradients result.

It is well known that large eddy simulation (LES) technique, which is much cheaper than the DNS since it solves only the large-scale components of turbulent flow and models the subgrid-scales (SGS) effects via SGS models, provides an effective tool to study some detailed features of turbulent flows. The SGS model is a key problem in the LES. A dynamic SGS model was proposed by Germano et al. [6] which overcome some shortcomings of the classical Smagorinsky model [7]. The dynamic model gained a remarkable success in the past decade and gave a new impetus to the development of new strategies for LES. In the present authors' group, the dynamic SGS models, including subgrid turbulent stress and heat flux models, were proposed and applied to stably and unstably stratified turbulent channel flows [8,9]. Recently, Garg et al. [10] performed the LES of stably stratified turbulent channel flow. The Boussinesq form of the governing equations was used and a dynamic eddy viscosity model was employed for the parameterization of the SGS stresses and density fluxes.

Armenio and Sarkar [11] performed an investigation of stably stratified turbulent channel flow with moderate-to-large levels of stratification to exhibit internal wave activity in the core of the channel.

Even though oscillating turbulent boundary layers have been extensively studied [12,13], statistically unsteady turbulent flows driven by time-varying force, e.g., time-varying buoyancy force considered here, have received little attention compared to statistically steady ones. Lu et al. [14] performed the LES for an oscillating flow past a circular cylinder. Then, Hsu et al. [15] dealt with an oscillating turbulent flow over a flat plate and verified that the LES approach coupled with the dynamic SGS model is suited to tackle unsteady problem. Scotti and Piomelli [16] investigated pulsating turbulent channel flow driven by oscillating pressure gradient and demonstrated that the LES can reasonably predict unsteady turbulence behavior. Recently, Wang and Lu [17] studied turbulent heat transfer in an oscillating turbulent channel flow by use of LES technique.

In this study, LES is employed to investigate thermally stratified turbulent channel flow with temperature oscillation on the bottom wall of the channel at different Richardson numbers and oscillation periods. The three-dimensional resolved incompressible Navier–Stokes and energy equations are solved by the fractional-step method proposed by Verzicco and Orlandi [18]. Dynamic SGS models of turbulent stress and turbulent heat flux are used.

This paper is organized as follows. The mathematical formulations and the dynamic SGS models for modeling turbulent stresses and heat fluxes are described in Section 2. The numerical methods and validation are given in Section 3. In Section 4, some quantities including the phase-averaged resolved velocities, temperature and their fluctuations and turbulent heat flux, and turbulence structures based on instantaneous velocity and temperature fluctuations are discussed. Finally, concluding remarks are summarized in Section 5.

2. Mathematical formulations

Thermally stratified turbulent channel flow with temperature oscillation on the bottom wall is considered. The temperature on the upper wall (T_U) is maintained as a constant and chosen as $T_U = 0$, and the temperature on the bottom wall (T_B) is subjected to vary sinusoidally about zero with an amplitude ΔT. The governing equations are the three-dimensional filtered incompressible Navier–Stokes and the energy equations under the Boussinesq approximation based on a tophat filter. To non-dimensionalize the governing equations, the half-height of the channel δ is used as the length scale, the friction velocity u_τ of unstratified shear turbulent channel flow as the velocity scale, and the amplitude of oscillating temperature on the bottom wall ΔT as the temperature scale. The non-dimensional governing equations are then given as,

$$\frac{\partial \bar{u}_i}{\partial x_i} = 0 \tag{1}$$

$$\frac{\partial \bar{u}_i}{\partial t} + \frac{\partial}{\partial x_j}(\bar{u}_i \bar{u}_j) = -\frac{\partial \bar{p}}{\partial x_i} + \frac{1}{Re_\tau}\frac{\partial^2 \bar{u}_i}{\partial x_j \partial x_j} - \frac{\partial \tau_{ij}}{\partial x_j} + \delta_{i1} + Ri_\tau \widetilde{\overline{T}}\,\delta_{i2} \tag{2}$$

$$\frac{\partial \overline{T}}{\partial t} + \frac{\partial(\overline{T}\bar{u}_j)}{\partial x_j} = \frac{1}{Re_\tau Pr}\frac{\partial^2 \overline{T}}{\partial x_j \partial x_j} - \frac{\partial q_j}{\partial x_j} \tag{3}$$

$$\tau_{ij} = R_{ij} - \delta_{ij}R_{kk}/3, \quad R_{ij} = \overline{u_i u_j} - \bar{u}_i \bar{u}_j;$$
$$q_j = \overline{T u_j} - \overline{T}\bar{u}_j \tag{4}$$

where the "overbar" denotes the filtered variables, $\bar{u}_i$ ($i = 1, 2, 3$), corresponding to u, v, w, represents the resolved velocity components in the streamwise (x), wall-normal (y) and spanwise (z) directions, respectively. $\bar{p}$ is the resolved pressure plus $R_{kk}/3$. The fixed streamwise pressure gradient is accounted for by the term δ_{i1} in Eq. (2). $\widetilde{\overline{T}} = \overline{T} - \langle \overline{T} \rangle_S$, and $\langle\ \rangle_S$ stands for an average over a plane parallel to the horizontal walls. $Re_\tau = u_\tau \delta/\nu$ represents the Reynolds number and $Pr = \nu/\kappa$ is the molecular Prandtl number with ν being the kinematic viscosity of the fluid and κ, the thermal diffusivity. Ri_τ is the Richardson number defined as $Ri_\tau = \beta g \Delta T \delta/u_\tau^2$, where β is the thermal expansion coefficient which assumed small enough so that the Boussinesq approximation is applicable, and g is the gravitational acceleration. Usually, the Richardson number Ri_τ is used to characterize buoyancy effect in stably or unstably stratified channel flow. Here, it also represents a reference parameter with maximum temperature difference on both the walls when the temperature on the bottom wall is forced to vary with time.

In Eqs. (2) and (3), τ_{ij} and q_j represent SGS turbulent stress and heat flux, respectively, which need to be modeled by SGS models. The overall expressions of the SGS stresses and turbulent heat flux are read as

$$\tau_{ij} = -2C\overline{\Delta}^2 |\overline{S}|\overline{S}_{ij}, \quad q_j = -\frac{C\overline{\Delta}^2}{Pr_T}|\overline{S}|\frac{\partial \overline{T}}{\partial x_j} \tag{5}$$

where $\overline{S}_{ij} = (\partial \bar{u}_i/\partial x_j + \partial \bar{u}_j/\partial x_i)/2$, $|\overline{S}| = [2\overline{S}_{ij}\overline{S}_{ij}]^{\frac{1}{2}}$. Pr_T represents the turbulent Prandtl number. $\overline{\Delta}$ is the filter width, as proposed by Germano et al. [6], is defined as $\overline{\Delta} = (\Delta_1 \Delta_2 \Delta_3)^{1/2}$ with Δ_j ($j = 1, 2, 3$) being the grid spacing in the j direction.

The model coefficients of C and Pr_T in Eq. (5) are obtained by the approach proposed by Germano et al. [6]. After introducing a test filtering (i.e., a tophat filter considered here) with a filter width $\widehat{\overline{\Delta}}$ to Eqs. (1)–(3),

the coefficients C and Pr_T can be dynamically determined as

$$C = -\frac{1}{\overline{\Delta}^2}\frac{\langle L_{ij}M_{ij}\rangle_S}{\langle M_{ij}M_{ij}\rangle_S}, \quad Pr_T = -C\overline{\Delta}^2\frac{\langle F_iF_i\rangle_S}{\langle E_iF_i\rangle_S} \tag{6}$$

where $M_{ij} = 2\alpha^2\left|\widehat{\overline{S}}\right|\left[\widehat{\overline{S}}_{ij} - \frac{1}{3}\widehat{\overline{S}}_{kk}\delta_{ij}\right] - \hat{m}_{ij}$, $L_{ij} = \hat{\bar{u}}_i\hat{\bar{u}}_j - \hat{\bar{u}}_i\hat{\bar{u}}_j - \frac{1}{3}(\hat{\bar{u}}_k\hat{\bar{u}}_k - \hat{\bar{u}}_k\hat{\bar{u}}_k)\delta_{ij}$, $m_{ij} = 2|\overline{S}|\left[\overline{S}_{ij} - \frac{1}{3}\overline{S}_{kk}\delta_{ij}\right]$, $E_i = \hat{\bar{u}}_i\widehat{\overline{T}} - \hat{\bar{u}}_i\overline{T}$, $F_i = \alpha^2|\widehat{\overline{S}}|\widehat{\overline{B}}|_i - |\overline{S}|\hat{B}_i$, and $B_j = \frac{\partial\overline{T}}{\partial x_j}$.

Here, $\alpha = \widehat{\overline{\Delta}}/\overline{\Delta}$ is chosen as 2 in the present calculation. The spatial average of $\langle\ \rangle_S$ in Eq. (6) is to remove the calculation oscillation [6]. It is still needed to note that the validity of the dynamic SGS models to study statistically unsteady turbulent flow has been established by performing detailed validation and verification in [15–17].

No-slip and no-penetration velocity conditions are imposed on the walls. Periodic boundary conditions are employed in the streamwise and spanwise directions. After a fully developed turbulent channel flow is established, a fixed temperature on the upper wall and an oscillating temperature on the bottom wall are imposed. Here, the non-dimensional temperature on the upper wall of the channel is $T_U = 0$, and the non-dimensional temperature on the bottom wall represents $T_B = -\sin(2\pi t/t_P)$, where t_P represents the period of temperature oscillation.

3. Numerical methods and validation

A fractional-step method proposed by Verzicco and Orlandi [18] is employed to solve Eqs. (1)–(3). Spatial derivatives are discretized with a second order central difference on a staggered grid for all the terms in the equations. Time advancement is carried out by the semi-implicit scheme mixing the Crank–Nicolson scheme for the viscous terms and the third-order Runge–Kutta scheme for the convective terms. The low-storage Runge–Kutta methods have the additional advantage that the minimum amount of computer run-time memory is realized. The discretized formulation was described in detail by Verzicco and Orlandi [18].

The size of computational domain is $4\pi\delta \times 2\delta \times 2\pi\delta$ with the corresponding grid number $97\times97\times65$ in the streamwise, wall-normal and spanwise directions. The computational domain size is chosen such that two-point correlations in the streamwise and spanwise directions are negligibly small. The grid is uniform along both the streamwise and spanwise directions. In the wall-normal direction, to increase the grid resolution near both the walls, the mesh is stretched following the transformation used in [19,20], so that the grid distribution in the wall-normal direction is sufficient to resolve the viscous sublayer and diffusive sublayer near the boundary.

To validate the present calculation procedure, some typical DNS results for stably and unstably stratified turbulent channel flow performed by Iida and coworkers [4,5] are used to compare with our results. Here, two typical cases for $Re_\tau = 150$ and $Ri_b = 0$ and 0.18 (or $Ri_\tau = 0$ and 12 approximately), where Ri_b is the Richardson number based on the bulk velocity of the turbulent channel flow, are employed to validate the present calculation. Fig. 1 shows the distributions of turbulent intensities normalized by the friction velocity and the temperature fluctuation normalized by the friction temperature. It is seen that our calculated results are in good agreement with the DNS data. Other turbulent quantities (not shown here) are also calculated and agree well with the DNS results. Based on recent investigation [21,22] for the effect of turbulence models and numerical errors in LES, the dynamic mixed SGS model [23] is also used to examine the influence of turbulence model in LES on the present calculated results. As shown in Fig. 1a, both the results calculated by the dynamic Smagorinsky model [6] and the dynamic mixed model [23] agree well each other; it is confirmed that the SGS model and grid resolution used in this study can accurately calculate the turbulent flow.

To ensure that the computed results are independent of the time steps and the grid sizes, results calculated by

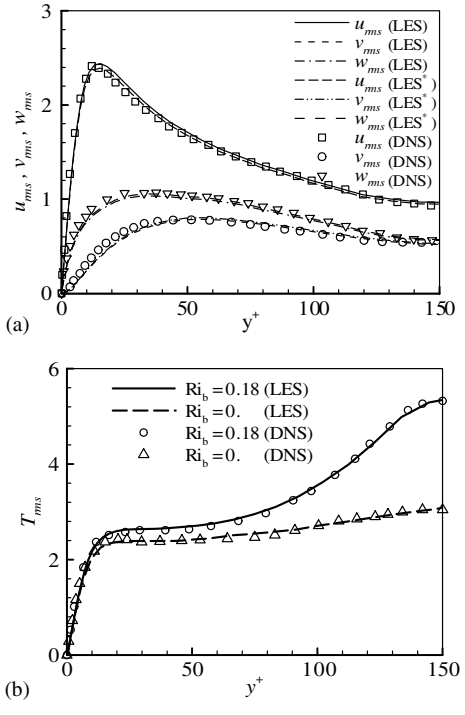

Fig. 1. Comparison of the present LES results with DNS data [5] for the turbulent intensities at $Ri_b = 0$ (a) and temperature fluctuation (b), where LES* represents the results calculated by the dynamic mixed SGS model.

different grid numbers and time steps were carefully examined in our previous study [24] and agree well each other (cf. Fig. 2 in [24]). Moreover, extensive validations and verifications have been performed in our previous work for unstably stratified turbulent channel flow [8,9], oscillating turbulent channel flow driven by unsteady external force [15], oscillating turbulent channel flow with heat transfer [17], and turbulent passive scalar transfer at high Prandtl number [20,24]. Thus, it can be confirmed that our calculation is reliable for the prediction of statistical quantities of thermally stratified turbulent shear flows.

4. Results and discussion

Calculations have been performed for $Ri_\tau = 0$, 50 and 128, $t_P = 3.2$ and 6.4, $Pr = 0.71$, and $Re_\tau = 180$. Due to inherent unsteadiness of the driving force, i.e., time-varying buoyancy force induced by the temperature oscillation, the phase-averaged statistical turbulent quantities are calculated by taking the average at the same phase and over the plane parallel to the wall. To remove initial effect, the phase-averaged statistical quantities are calculated in several oscillation periods after the initial influence has been swept.

4.1. Time evolution of resolved turbulent kinetic energy

The buoyancy force has a significant influence on the vertical turbulent transport and internal energy conversion between turbulent kinetic energy and turbulent potential energy. For thermally stratified shear turbulent channel flow with temperature oscillation on the wall, the turbulent channel flow is undergone by time-varying buoyancy force induced by the temperature variation. When the temperature on the bottom wall is lower (or higher) than that on the upper wall, the channel flow behaves similarly as stably (or unstably) stratified flow. Thus, as the temperature on the bottom wall is forced to vary with time in certain periods and amplitudes, stably and unstably stratified flow evolutions occur alternately in one cycle.

To reveal global character and statistically unsteady behavior of thermally stratified turbulent channel flow induced by the temperature oscillation on the bottom wall, as used by Garg et al. [10], the volume-integrated turbulent kinetic energy E_k is defined as

$$E_k = \frac{1}{2}\int_{-1}^{1} \langle (\bar{u}')^2 + (\bar{v}')^2 + (\bar{w}')^2 \rangle_S \mathrm{d}y \tag{7}$$

where $\bar{u}_i' = \bar{u}_i - \langle \bar{u}_i \rangle_S$. Then, Fig. 2 shows the time evolution of E_k and its phase-average (i.e., E_{kP}). The distribution of E_k for $Ri_\tau = 50$ and $t_P = 6.4$ and the corresponding sinusoidal curve of the temperature variation are shown in Fig. 2a. It is reasonably predicted that E_k varies quasi-periodically with time. By comparing with the phases corresponding to the lowest peaks of E_k and T_B, it is found that E_k changes with a phase lag about $t_P/4$ with respect to T_B. This behavior implies that the turbulent flow needs time to reflect the temperature variation on the wall.

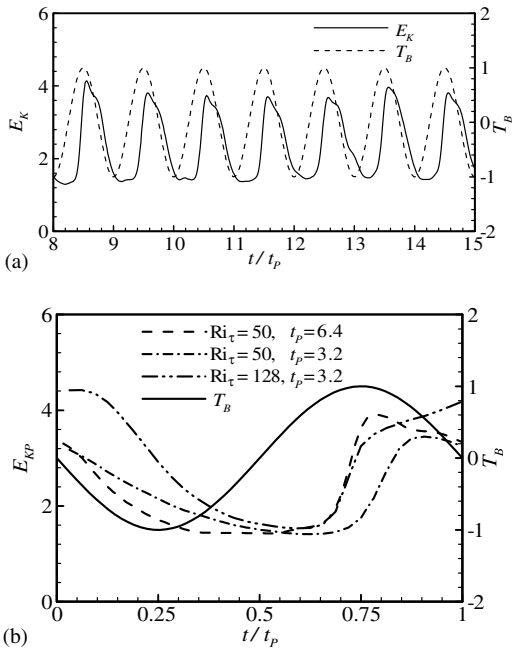

Fig. 2. Time evolution of the volume-integrated turbulent kinetic energy (E_k) and its phase-average (E_{kP}): (a) E_k, and (b) E_{kP}.

The phase-average value of E_k, denoted by E_{kP}, is depicted in Fig. 2b. By viewing the profile of $Ri_\tau = 50$ and $t_P = 6.4$, when the temperature on the bottom wall is lower than that on the upper wall during $0 < t/t_P < 1/2$, the turbulent channel flow behaves similarly as stable stratification and turbulence intensities are suppressed. Thus, E_{kP} decreases smoothly during $0 < t/t_P < 1/2$. When the temperature on the bottom wall is higher than that on the upper wall during $1/2 < t/t_P < 1$, the turbulent channel flow behaves as unstable stratification. As shown in Fig. 2b, E_{kP} increases gradually in $1/2 < t/t_P < 0.7$, then changes quickly to high value from $t/t_P = 0.7$ to 0.8 approximately, finally decreases asymptotically in $0.8 < t/t_P < 1$.

4.2. Phase-averaged velocity and temperature

Fig. 3 shows the profiles of the phase-averaged velocity for $Ri_\tau = 50$ and $t_P = 6.4$. The velocity profile evolution appears the tendency of re-laminarization

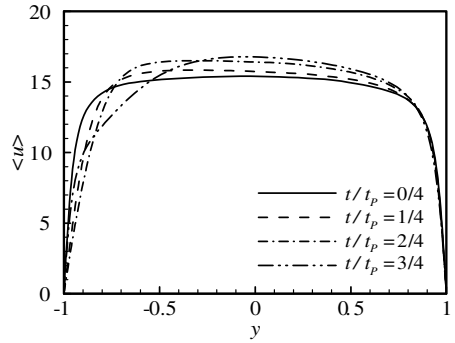

Fig. 3. Profiles of the phase-averaged velocity for $Ri_\tau = 50$ and $t_P = 6.4$.

from $t/t_P = 3/4$ through 4/4 (or 0/4) to 2/4 near the bottom wall. From the velocity profiles in logarithmic scale, it is found that the logarithmic region disappears whereas the linear sublayer is extended. Then, the velocity profile from $t/t_P = 2/4$ to 3/4 develops gradually to blunt distribution due to unstable stratification effect. The velocity profile at $t/t_P = 3/4$ exhibits that there exists a buffer layer followed by a logarithmic region after redrawing it using the logarithmic scale. This behavior is consistent with the variation of the resolved turbulent kinetic energy shown in Fig. 2 and with the previous work [8–11]. As the influence of time-varying buoyancy force, remarkable variation of the phase-averaged velocity occurs near the bottom wall, and the profiles of the velocity at different phases coincide closely each other near the upper wall with $y > 0.85$ approximately.

The profiles of the phase-averaged temperature are shown in Fig. 4 for $t_P = 6.4$, and $Ri_\tau = 50$ and 0. The profiles of the temperature vary obviously in the lower half-channel region. It is interesting to note that the phase-averaged temperature has a positive shift-value about 0.15 over the core region of $-0.5 < y < 0.8$ approximately in Fig. 4a. To examine the stratification effect on the mean temperature distribution, the profiles of the phase-averaged temperature for $Ri_\tau = 0$ (i.e., passive heat transfer) is shown in Fig. 4b, and approaches zero in the region of $-0.5 < y \leqslant 1.0$. Thus, the distinction in Fig. 4a and b shows that dynamic coupling effect of the turbulent flow and the temperature field results the shift-value of the mean temperature distribution for thermally stratified turbulent channel flow coupled with the temperature varying with time on the wall.

Fig. 4c shows the profile of the mean temperature (i.e., $\langle T\rangle_T$) calculated by taking the average over the plane parallel to the wall during the whole time region of several oscillation periods. The mean temperature profile for $Ri_\tau = 50$ and $t_P = 6.4$ depicts negative value near

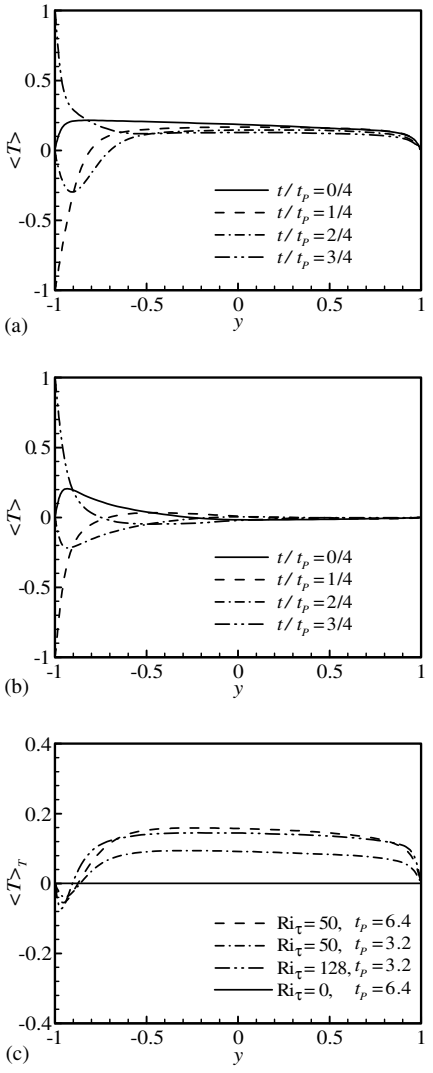

Fig. 4. Distributions of the phase-averaged and mean temperature. (a) Phase-averaged temperature for $Ri_\tau = 50$ and $t_P = 6.4$, (b) phase-averaged temperature for $Ri_\tau = 0$ and $t_P = 6.4$, and (c) whole time averaged temperature.

the bottom wall due to the influence of the forced temperature oscillation on the bottom wall. Then the mean temperature exhibits a plateau distribution over the most core region of the channel, and decreases gradually to zero at the upper wall. Meanwhile, it is reasonably predicted that the mean temperature distribution for $Ri_\tau = 0$ is zero over the channel.

4.3. Velocity and temperature fluctuations and heat fluxes

To examine the effect of the temperature oscillation on turbulence quantities, the velocity and temperature fluctuations are discussed. The temperature variation on

the bottom wall induces an oscillating thermal transfer that interacts with turbulent flow to produce a time-varying response to turbulence quantities. As turbulent flow is influenced by stable or unstable stratification, turbulence intensity is reduced and strengthened alternately in one cycle. Fig. 5 shows the profiles of the phase-averaged turbulent intensities for $Ri_\tau = 50$ and $t_P = 6.4$ at several phases. The corresponding turbulent intensities of unstratified turbulent channel flow at the same Reynolds number (referred to as $Ri_\tau = 0$) are also plotted in Fig. 5. The evolution of the streamwise turbulent intensity u_{rms} in one cycle is similar to that of turbulent kinetic energy in Fig. 2b. The profile of u_{rms} near the bottom wall decreases gradually from $t/t_P = 0/4$ to 2/4, and changes quickly to high level distribution at $t/t_P = 3/4$. According to the distributions of v_{rms} and w_{rms} in Fig. 5b and c, it can be concluded that the increase of E_{kP} from $t/t_P = 0.7$ to 0.8 in Fig. 2b is mainly contributed by u_{rms}.

The vertical turbulent intensity v_{rms} is shown in Fig. 5b. At $t/t_P = 1/4$ and 2/4, the distributions of v_{rms} for $Ri_\tau = 50$ are lower than that for $Ri_\tau = 0$ near the bottom wall due to stable stratification effect. This character is consistent with the previous work for stably stratified turbulent channel flows [8–11]. Then, the profiles of v_{rms} for $Ri_\tau = 50$ at $t/t_P = 3/4$ and 0/4 (or 4/4) are higher than the distributions of $Ri_\tau = 0$ due to unstable stratification effect. Note that the distributions of v_{rms} for $Ri_\tau = 50$ in the vicinity of the upper wall are higher than that for $Ri_\tau = 0$. It can be explained as locally unstable stratification effect, because, as shown in Fig. 4a and c, the mean temperature near the upper wall decreases gradually to zero and a negative temperature gradient is generated near the upper wall. Since the temperature gradient is parallel to the buoyancy force, the temperature oscillation directly influences the change of the vertical velocity fluctuation v_{rms}, then induces the variation of the horizontal components u_{rms} and w_{rms} through the resolved pressure–strain correlation which governs the exchange of energy among the three components. Thus, as shown in Fig. 5c, the variation of

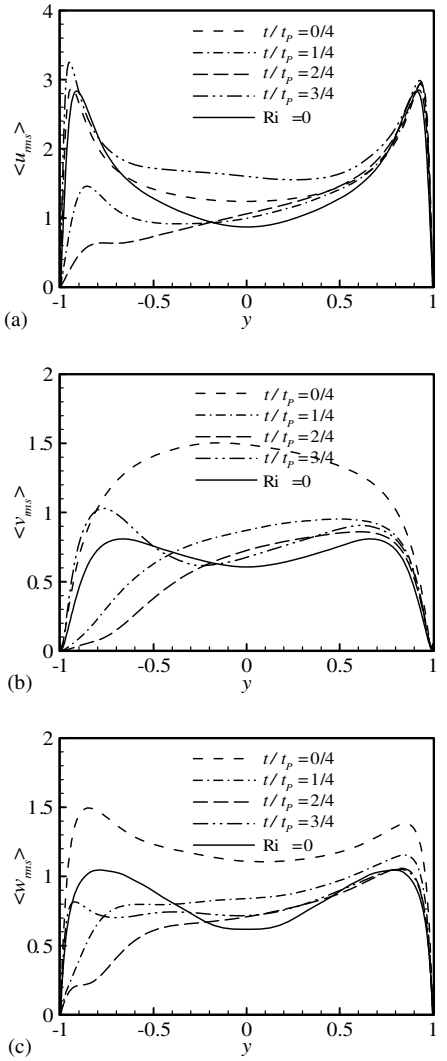

Fig. 5. Distributions of the phase-averaged turbulent intensities for $Ri_\tau = 50$ and $t_P = 6.4$: (a) u_{rms}, (b) v_{rms}, and (c) w_{rms}.

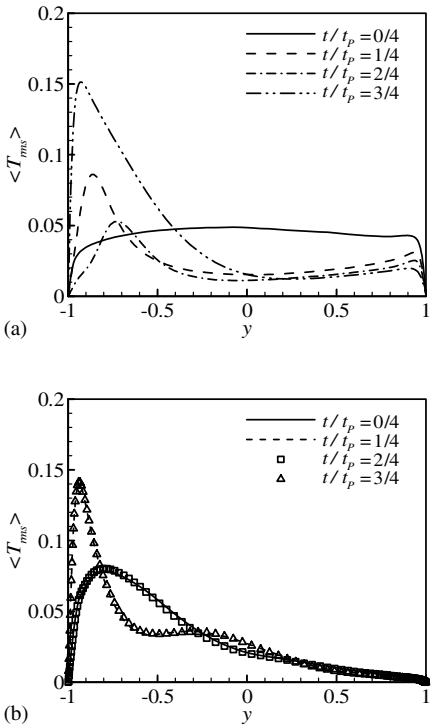

Fig. 6. Profiles of the phase-averaged temperature fluctuation. (a) $Ri_\tau = 50$ and $t_P = 6.4$, and (b) $Ri_\tau = 0$ and $t_P = 6.4$.

spanwise turbulent intensity w_{rms} is similar to that of v_{rms} during the cycle.

Fig. 6 shows the distributions of the temperature fluctuation (T_{rms}). As shown in Fig. 6a for $Ri_\tau = 50$ and $t_P = 6.4$, the temperature fluctuation exhibits a plateau distribution over the most core region at $t/t_P = 0/4$. Then a peak of T_{rms} is formed in the vicinity of the bottom wall. The position of the peak moves away from the bottom wall as the peak value of T_{rms} decreases. At $t/t_P = 3/4$, a highest peak occurs. The profiles of T_{rms} for $Ri_\tau = 0$ are also illustrated in Fig. 6b, as expected, coincide together for $t/t_P = 0/4$ and 2/4 (or for $t/t_P = 1/4$ and 3/4). Compared to Fig. 6b, the temperature fluctuation T_{rms} for $Ri_\tau = 50$ is reduced and strengthened alternately near the bottom wall due to the significant influence of the temperature oscillation. Meanwhile, as the locally unstable stratification effect induced by the negative mean temperature gradient near the upper wall, the peaks with small values for T_{rms} appear at several phases for $Ri_\tau = 50$ in Fig. 6a, however, T_{rms} approaches zero asymptotically with $y \to 1$ for $Ri_\tau = 0$ in Fig. 6b.

Fig. 7 shows the profiles of the vertical and streamwise heat fluxes (i.e.,$\langle T'v' \rangle$ and $\langle T'u' \rangle$) at several phases. In Fig. 7a and b for $Ri_\tau = 50$ and $t_P = 6.4$, the vertical and streamwise heat fluxes demonstrate significant change near the bottom wall at different phases. In Fig. 7c and d for $Ri = 0$, the profiles of $\langle T'v' \rangle$ and $\langle T'u' \rangle$ for $t/t_P = 0/4$ and 2/4 (or for $t/t_P = 1/4$ and 3/4) exhibit antisymmetric distribution. Compared to the distributions in Fig. 7c and d, the vertical heat flux $\langle T'v' \rangle$ for $Ri_\tau = 50$ is reduced at $t/t_P = 1/4$ and 2/4, and strengthened at $t/t_P = 3/4$ and 0/4 (or 4/4) near the bottom wall. Due to locally unstable stratification effect near the upper wall, the profiles of $\langle T'u' \rangle$ depict small peaks there at several phases.

The term contributed by the buoyancy force in the budget transport equations of the resolved turbulent kinetic energy (i.e., $\langle u_i' u_i' \rangle$) and the resolved wall-normal Reynolds stress (i.e., $\langle u_2' u_2' \rangle$, or $\langle v'v' \rangle$) can be written as $2Ri_\tau \langle T'v' \rangle$. Thus, the profiles in Fig. 7a, when multiplied by $2Ri_\tau$, represent the budget term induced by the buoyancy force. Combining with Fig. 5b, it is reasonably to find that the $\langle T'v' \rangle$ in Fig. 7a contributes high level distribution of v_{rms} in Fig. 5b at $t/t_P = 0/4$. The values of $\langle T'v' \rangle$ are relatively small and the v_{rms} exhibits lower distributions near the bottom wall at $t/t_P = 1/4$ and 2/4. Meanwhile, the profile of $\langle T'v' \rangle$ with small value at $t/t_P = 1/4$ and 2/4 corresponds to lower distribution of E_{kP} for $Ri_\tau = 50$ and $t_P = 6.4$ in Fig. 2b, indicating that turbulent kinetic energy is suppressed due to stable stratification. Then, the $\langle T'v' \rangle$ increases in the vicinity of the bottom wall at $t/t_P = 3/4$, correspondingly v_{rms} increases in Fig. 5b. Thus, this budget term (i.e.,

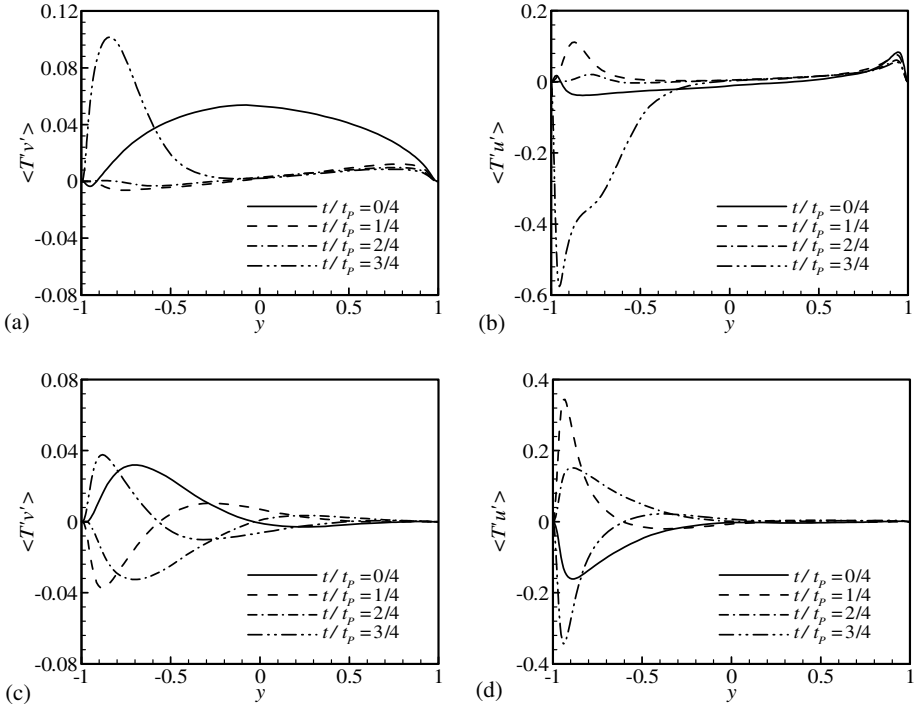

Fig. 7. Distributions of the vertical and streamwise heat fluxes. (a) $\langle T'v' \rangle$, (b) $\langle T'u' \rangle$ for $Ri_\tau = 50$ and $t_P = 6.4$, (c) $\langle T'v' \rangle$, and (d) $\langle T'u' \rangle$ for $Ri_\tau = 0$ and $t_P = 6.4$.

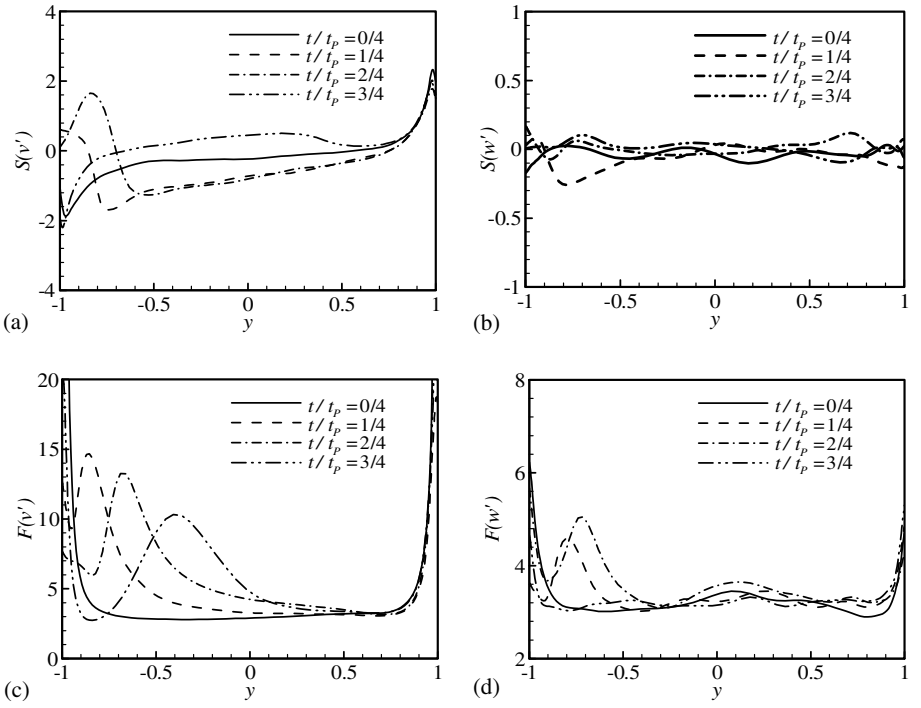

Fig. 8. Skewness and flatness factors of the velocity fluctuations. (a) $S(v')$, (b) $S(w')$, (c) $F(v')$, and (d) $F(w')$.

$2Ri_\tau\langle T'v'\rangle$) reasonably predicts the evolution of the vertical turbulent intensity.

The skewness and flatness factors of the velocity fluctuations at several phases are plotted in Fig. 8. The skewness factor of the wall-normal velocity fluctuation $S(v')$ is positive near the upper wall for all phases in Fig. 8a. Correspondingly, $S(v')$ is negative near the bottom wall at $t/t_P = 3/4$ and 0/4, representing the large-amplitude wall-normal velocity fluctuations due to arrival of high-speed fluid from regions away from the wall. $S(v')$ is positive near the bottom wall at $t/t_P = 1/4$ and 2/4, indicating the large-amplitude wall-normal velocity fluctuations probably associated low-speed fluid leaving the wall region. The skewness factor of the spanwise velocity fluctuation $S(w')$ is approximately equal to zero over the channel in Fig. 8b, which corresponds to the skewness factor of a Gaussian distribution. In Fig. 8c and d, the flatness factors of the wall-normal velocity fluctuation $F(v')$ and the spanwise velocity fluctuation $F(w')$ reach their maximum at both the walls, and form secondary peak near the bottom wall at different positions. In particular for $F(v')$ in Fig. 8c, it is interesting to note that the position of the peak moves away from the bottom wall and the value of $F(v')$ decreases from $t/t_P = 1/4$ to 3/4. Thus, it is reasonable to predict that the change of the flatness factors indicates that turbulence is highly intermittent in the near bottom wall region because of the influence of the temperature oscillation on the bottom wall.

4.4. Structures of turbulent flow and temperature

To get better insight into the flow structures, some typical instantaneous flow patterns are visualized. Fig. 9 shows the instantaneous contours of the wall-normal velocity fluctuation at several phases, in a plane parallel to the wall at $y^+ = 20$. The patterns clearly illustrate the evolution of turbulent intensities with absent and healthy streaky structures at different phases. At $t/t_P = 3/4$ and 0/4 (or 4/4), fairly healthy streaky structures can be observed, corresponding to the strengthened vertical turbulent intensity shown in Fig. 5b. At $t/t_P = 3/4$, very long streaks generate with respect to $t/t_P = 0/4$. This phenomenon is related to the energy transfer between the wall-normal and horizontal directions based on the analysis of the Reynolds-stress budgets [19]. As stable stratification effect plays as a dominating factor from $t/t_P = 1/4$ to 2/4, turbulence is significantly suppressed and the absent streaky structures appear. Then, the vertical turbulent intensity increases gradually from $t/t_P = 2/4$ and is significantly strengthened at $t/t_P = 3/4$. The evolution shown in Fig. 9 is well consistent with the previous observations [8,9] as well as with the development of the vertical turbulent intensity given in Fig. 5b.

The instantaneous patterns of the streamwise velocity fluctuation and the temperature fluctuation during one cycle (not shown here) are also observed at the same plane as plotted in Fig. 9. It is found that the

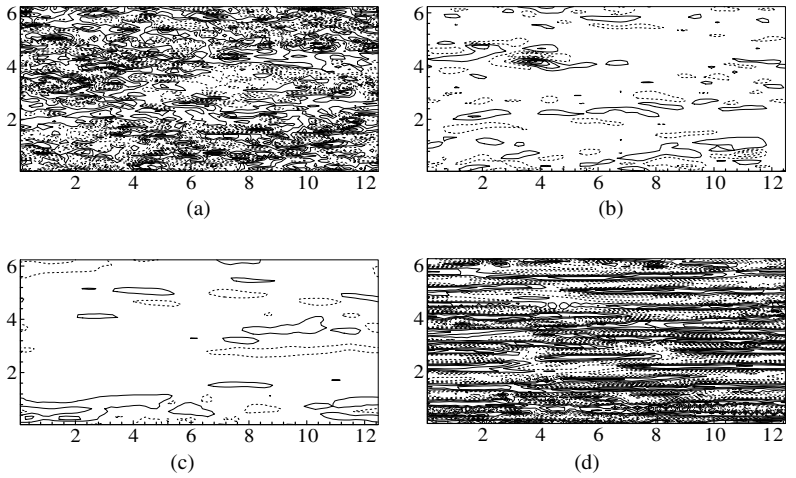

Fig. 9. Instantaneous contours of the wall-normal velocity fluctuation in a x–z plane at $y^+ = 20$. (a) $t/t_P = 0/4$, (b) 1/4, (c) 2/4, and (d) 3/4.

well-known low- and high-speed streaks are clearly illustrated and the local hot spots in accordance with the high- and low-temperature regions are identified. These observations imply that the turbulent mixing of temperature is controlled by the turbulence dynamics in the near wall regions. Meanwhile, the time development of the instantaneous streamwise velocity fluctuation and temperature fluctuation at different phases agrees well with the phase-averaged quantities in Figs. 5a and 6a, respectively.

The contours of the temperature fluctuation in the vertical cross-section in the vicinity of the bottom wall are shown in Fig. 10. The streaky structures clearly demonstrate the development of the temperature fluctuation and are well consistent with the distributions of the temperature fluctuation given in Fig. 6a. At $t/t_P = 0/4$, the streaky structures spread over the channel in Fig. 10a, corresponding to a plateau distribution of T_{rms} in Fig. 6a. At $t/t_P = 1/4$, the organized streaks of the temperature fluctuation mainly distribute over the region about $y = -0.75$ in Fig. 10b, and a peak of T_{rms} occurs at the same location in Fig. 6a. As the temperature on the bottom wall is zero at $t/t_P = 2/4$, the temperature fluctuation intensity becomes weaken. Finally, very healthy streaky structures can be observed near the bottom wall at $t/t_P = 3/4$ (Fig. 10d), and strong temperature fluctuation intensity also appears in Fig. 6a at the same phase.

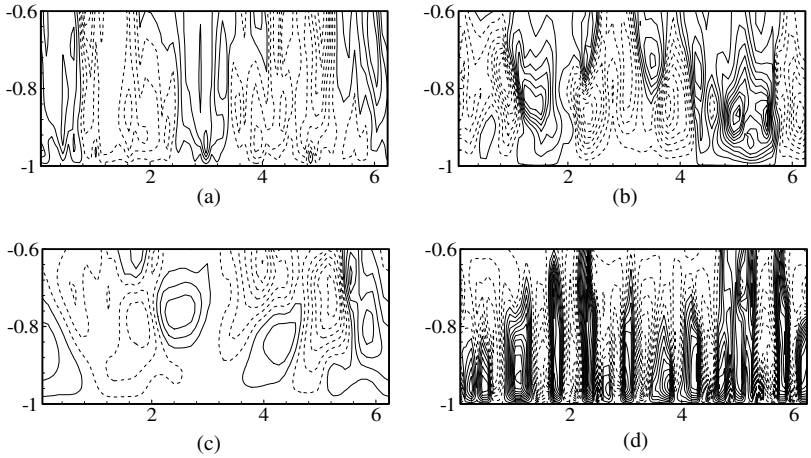

Fig. 10. Instantaneous contours of the temperature fluctuation in the vertical cross-section (i.e., z–y plane) in the vicinity of the bottom wall. (a) $t/t_P = 0/4$, (b) 1/4, (c) 2/4, and (d) 3/4.

4.5. Effect of Richardson number and oscillation period on turbulent flow and temperature

As well known, thermal stratification effect becomes more significant with the increase of the Richardson number. Meanwhile, when the period of oscillation is large (at a limit case $t_P \to \infty$, i.e., quasi-steady regime), as proposed by Binder et al. [25], the turbulence has enough time to relax to the local equilibrium for approaching fully developed turbulent flow. Thus, it is interesting to examine the effect of the Richardson number and the period of oscillation on the thermally stratified turbulent flows. Here, the parameters are chosen as the Richardson number $Ri_\tau = 0$, 50 and 128, the period of oscillation $t_P = 3.2$ and 6.4, and typical results are briefly discussed.

Fig. 2b shows the profiles of the volume-integrated turbulent kinetic energy. It is found that the phase difference between E_{kP} and T_B is somewhat different for three cases. E_{kP} decreases gradually for these cases because the turbulent channel flow behavior is similar to thermally stable stratified flow in $0 < t/t_P < 1/2$. Then, E_{kP} changes smoothly in $1/2 < t/t_P < 0.7$, and increases quickly from $t/t_P = 07$ to 0.8 approximately. It is reasonably predicted that the amplitude of E_{kP} at $Ri_\tau = 128$ is larger than that at $Ri_\tau = 50$.

Fig. 4c shows the profiles of the time–mean temperature for these cases. The mean temperature profiles exhibit small negative values near the bottom wall due to the influence of the forced temperature oscillation. Then, the plateau distributions with positive shift-values over the most core region of the channel are observed, and the shift-value of the mean temperature increases with the increase of the Richardson number and/or the period of oscillation. It represents that the dynamic coupling effect between the turbulent flow and the temperature field is strengthened with increasing the Richardson number and the period of oscillation.

To investigate the influence of the Richardson number and the period of oscillation on the velocity fluctuation, the distributions of the wall-normal velocity fluctuation (v_{rms}) are shown in Fig. 11. Similar to the profiles in Fig. 5b, the distributions of v_{rms} at $t/t_P = 1/4$ and 2/4 for the cases of $Ri_\tau = 50$ and 128 are lower than these for $Ri_\tau = 0$ near the bottom wall. During $1/2 < t/t_P < 1$, the turbulent channel flow behavior is similar to unstably stratified flow and turbulence intensities are strengthened. Thus, as shown typically in Fig. 11a and b, the profiles of v_{rms} at $t/t_P = 3/4$ and 0/4 (or 4/4) for $Ri_\tau = 50$ and 128 are larger than the distributions for $Ri_\tau = 0$ in the most core region. Meanwhile, the vertical turbulent intensity increases with increasing the Richardson number and/or the period of oscillation during $1/2 < t/t_P < 1$.

The distributions of the temperature fluctuation (T_{rms}) are shown in Fig. 11c and d, typically, at

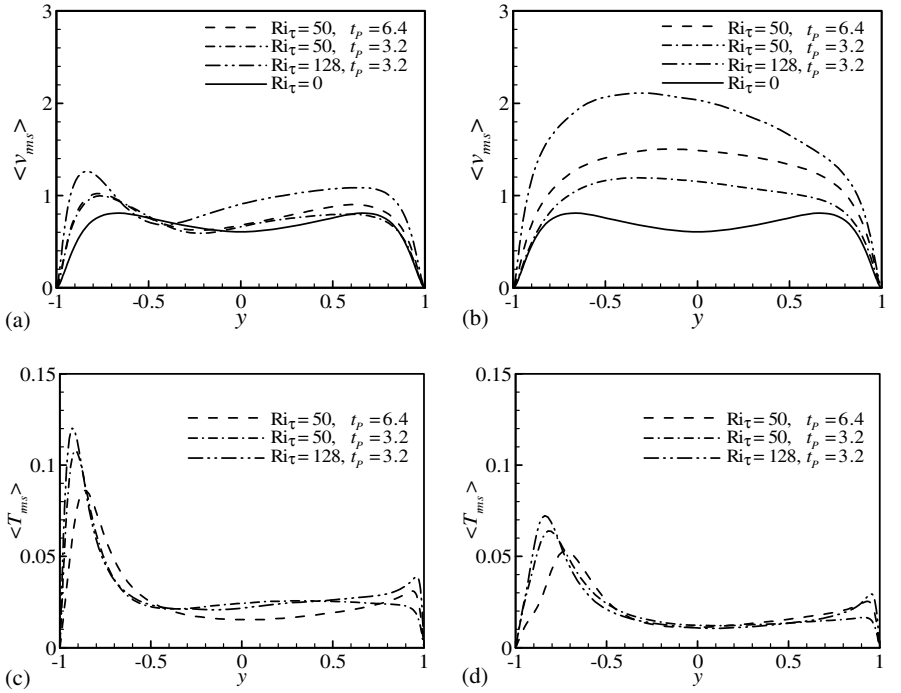

Fig. 11. Distributions of the wall-normal velocity fluctuation (v_{rms}) and the temperature fluctuation (T_{rms}) for different Richardson numbers and oscillating periods. (a) v_{rms} at $t/t_P = 3/4$, (b) v_{rms} at $t/t_P = 0/4$ (or 4/4), (c) T_{rms} at $t/t_P = 1/4$, and (d) T_{rms} at $t/t_P = 2/4$.

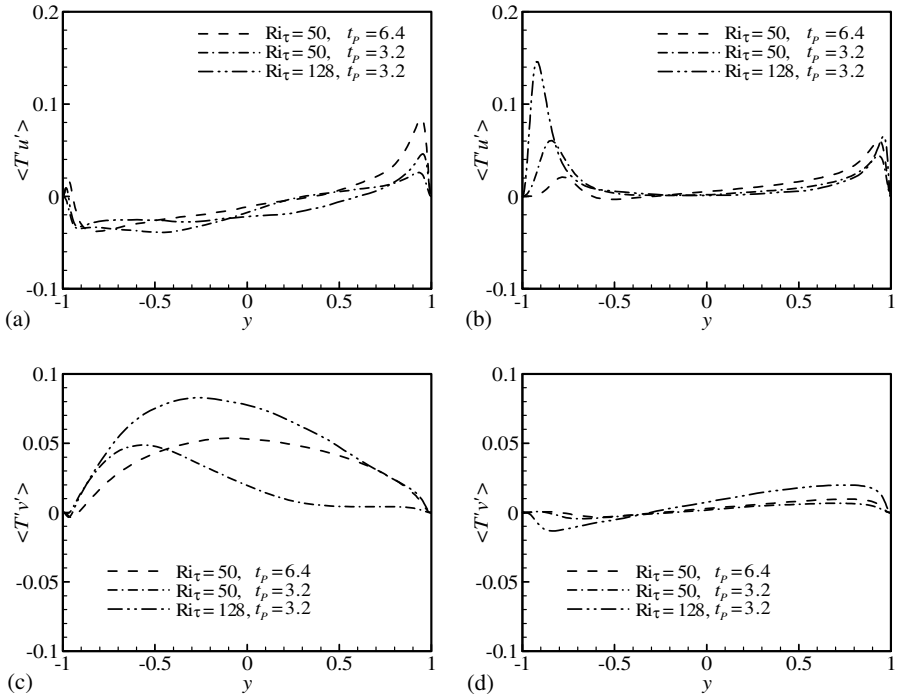

Fig. 12. Distributions of the vertical and streamwise heat fluxes for different Richardson numbers and oscillating periods. (a) $\langle T'u' \rangle$ at $t/t_P = 0/4$, (b) $\langle T'u' \rangle$ at $t/t_P = 2/4$, (c) $\langle T'v' \rangle$ at $t/t_P = 0/4$, and (d) $\langle T'v' \rangle$ at $t/t_P = 2/4$.

$t/t_P = 1/4$ and 2/4. The peaks of T_{rms} are formed in the vicinity of the bottom wall, and the position of the peak moves away from the bottom wall as the value of T_{rms} decreases. As discussed above, the turbulent channel flow character is similar to stably stratified flow at $t/t_P = 1/4$ and 2/4. The peak value of T_{rms} near the bottom wall increases with increasing the Richardson number. This behavior is consistent with the previous prediction for stably stratified turbulent channel flow [10,11]. As proposed by Binder et al. [25], when the period of the oscillation increases, turbulence intensity (or turbulent kinetic energy) is strengthened. Thus, due to the mechanism of internal energy conversion between turbulent kinetic energy and potential energy, the peak value of T_{rms} at $t_P = 3.2$ and $Ri_\tau = 50$ is reasonably higher than that at $t_P = 6.4$ in Fig. 11c and d. Correspondingly, based on the calculated results at $t/t_P = 1/4$ and 2/4 (not shown here), the peak value of v_{rms} at $t_P = 3.2$ and $Ri_\tau = 50$ is somewhat lower than that at $t_P = 6.4$.

Fig. 12 shows the profiles of the vertical and streamwise heat fluxes (i.e.,$\langle T'v' \rangle$ and $\langle T'u' \rangle$) at $t/t_P = 0/4$ and 2/4. In Fig. 12a and b, due to locally unstable stratification effect in the vicinity of the upper wall, the $\langle T'u' \rangle$ profile depicts small peak there. At $t/t_P = 0/4$, due to the influence of unstable stratification, the profiles of $\langle T'u' \rangle$ are negative near the bottom wall and the distributions of $\langle T'v' \rangle$ are positive. However, at $t/t_P = 2/4$, as the effect of stable stratification, the opposite behavior appears with respect to the profiles of $\langle T'v' \rangle$ and $\langle T'u' \rangle$ at $t/t_P = 0/4$. As discussed above, $\langle T'v' \rangle$ also reflects the effect of the buoyancy force on the budgets of the resolved turbulent kinetic energy. Thus, the effect of the buoyancy force becomes more important with the increase of the Richardson number and/or the period of oscillation, as shown in Fig. 12c and d.

5. Concluding remarks

Thermally stratified turbulent channel flow with temperature oscillation on the bottom wall of the channel has been investigated by use of large eddy simulation for the Richardson number $Ri_\tau = 0$, 50 and 128, the period of oscillation $t_P = 3.2$ and 6.4, the Prandtl number $Pr = 0.71$, and the Reynolds number $Re_\tau = 180$. Statistical turbulence quantities including the phase-averaged velocity, temperature and their fluctuations, turbulent heat fluxes, and the structures of turbulent flow and temperature are obtained to examine the effect of temperature oscillation on characteristics of thermally stratified turbulent channel flow.

When the temperature oscillation is forced on the bottom wall, the turbulent channel flow is affected by the time-varying buoyancy force and behaves similarly as stably and unstably stratified flow alternately. Based on

our calculated results, it is reasonably predicted that the tendency of re-laminarization and the enhancement of turbulent flow in the region near the bottom wall appear alternately during the cycle. According to the evolution of the volume-integrated turbulent kinetic energy, it varies quasi-periodically with a phase lag with respect to the temperature variation. It implies that the turbulent flow needs time to reflect the temperature oscillation on the wall. The phase difference between turbulent kinetic energy and the temperature oscillation is somewhat different for different Richardson numbers and oscillation periods.

As the dynamic coupling effect between turbulent flow and temperature field, the profile of the mean and phase-averaged temperature exhibits a plateau distribution with a positive shift-value over the most core region of the channel. The shift-value of the mean temperature increases with the increase of the Richardson number and/or the period of oscillation. Turbulent heat fluxes are calculated to exhibit their variation during the cycle, in particular for the wall-normal heat transfer which is closely related to the budget term contributed by the buoyancy force in the transport equation of the resolved turbulent kinetic energy. The budget term due to the time-varying buoyancy force quite well predicts the evolution of statistically unsteady turbulence intensity, and the effect of the buoyancy force becomes more important with the increase of the Richardson number and/or the period of oscillation.

The instantaneous patterns of the velocity and temperature fluctuations clearly demonstrate the structures of turbulent flow and temperature varying with time and are well consistent with the distributions of the corresponding statistical quantities along the wall-normal direction. These observations imply that the turbulent heat transfer is controlled by the turbulence dynamics in the near wall regions, in particular near the bottom wall on which the temperature oscillation is forced.

Acknowledgements

The authors are grateful to Professor L.X. Zhuang for helpful comments and discussion. This work was supported by the National Science Fund for Distinguished Scholars (no. 10125210), the China NKBRSF Project (no. 2001CB409600), the Programme of Hundred-Talent of the Chinese Academy of Sciences, and Specialized Research Fund for the Doctoral Program of Higher Education (no. 20020358013).

References

[1] P. Orlandi, Fluid Flow Phenomena, Kluwer Academic Publishers, 2002.

[2] J.I. Rohr, E.C. Itsweire, K.N. Helland, C.W. Van Atta, Growth and decay of turbulence in a stably stratified shear flow, J. Fluid Mech. 195 (1988) 77–111.

[3] T. Gerz, U. Schumann, S.E. Elghobashi, Direct numerical simulation of stratified homogeneous turbulent shear flows, J. Fluid Mech. 200 (1989) 563–594.

[4] O. Iida, N. Kasagi, Direct numerical simulation of unstably stratified turbulent channel flow, ASME J. Heat Transfer 119 (1997) 53–61.

[5] O. Iida, N. Kasagi, Y. Nagano, Direct numerical simulation of turbulent channel flow under stable stratification, Int. J. Heat Mass Transfer 45 (2002) 1693–1703.

[6] M. Germano, U. Piomelli, P. Moin, W. Cabot, A dynamic subgrid-scale eddy viscosity model, Phys. Fluids 3 (1991) 1760–1765.

[7] J. Smagorinsky, General circulation experiments with the primitive equations. I. The basic experiment, Mon. Weather Rev. 91 (1963) 99–165.

[8] N.Y. Liu, X.Y. Lu, L.X. Zhuang, A new dynamic subgrid-scale model for the large eddy simulation of stratified turbulent flows, Sci. China A 43 (2000) 391–399.

[9] F.Q. Zhong, N.S. Liu, X.Y. Lu, L.X. Zhuang, An improved dynamic subgrid-scale model for the large eddy simulation of stratified channel flow, Sci. China A 45 (2002) 888–899.

[10] R.P. Garg, J.H. Ferziger, S.G. Monismith, J.R. Koseff, Stably stratified turbulent channel flows. I. Stratification regimes and turbulence suppression mechanism, Phys. Fluids 12 (2000) 2569–2594.

[11] V. Armenio, S. Sarkar, An investigation of stably-stratified turbulent channel flow using large eddy simulation, J. Fluid Mech. 459 (2002) 1–42.

[12] S. Tardu, G. Binder, R.F. Blackwelder, Turbulent channel flow with large-amplitude velocity oscillations, J. Fluid Mech. 267 (1994) 109–151.

[13] C.R. Lodahl, B.M. Sumer, J. Fredsoe, Turbulent combined oscillatory flow and current in a pipe, J. Fluid Mech. 373 (1998) 313–348.

[14] X.Y. Lu, C. Dalton, J. Zhang, Application of large eddy simulation to an oscillating flow past a circular cylinder, ASME J. Fluids Eng. 119 (1997) 519–525.

[15] C.T. Hsu, X.Y. Lu, M.K. Kwan, LES and RANS studies of oscillating flows over a flat plate, ASCE J. Eng. Mech. 126 (2000) 186–193.

[16] A. Scotti, U. Piomelli, Numerical simulation of pulsating turbulent channel flow, Phys. Fluids 13 (2001) 1367–1384.

[17] L. Wang, X.Y. Lu, An investigation of turbulent oscillatory heat transfer in channel flows by large eddy simulation, Int. J. Heat Mass Transfer, in press.

[18] R. Verzicco, P. Orlandi, A finite-difference scheme for three-dimensional incompressible flows in cylindrical coordinates, J. Comput. Phys. 123 (1996) 402–414.

[19] P. Moin, J. Kim, Numerical investigation of turbulent channel flow, J. Fluid Mech. 118 (1982) 341–377.

[20] Y.H. Dong, X.Y. Lu, L.X. Zhuang, Large eddy simulation of turbulent channel flow with mass transfer at high-Schmidt numbers, Int. J. Heat Mass Transfer 46 (2003) 1529–1539.

[21] J. Gullbrand, F.K. Chow, The effect of numerical errors and turbulence models in large-eddy simulations

of channel flow, with and without explicit filtering, J. Fluid Mech. 495 (2003) 323–341.
[22] F.K. Chow, P. Moin, A further study of numerical errors in large-eddy simulations, J. Comput. Phys. 184 (2003) 366–380.
[23] Y. Zang, R.L. Street, J.R. Koseff, A dynamic mixed subgrid-scale model and its application to turbulent recirculating flows, Phys. Fluids 5 (1993) 3186–3196.
[24] Y.H. Dong, X.Y. Lu, L.X. Zhuang, An investigation of Prandtl number effects on turbulent heat transfer in channel flows by large eddy simulation, Acta Mech. 159 (2002) 39–51.
[25] G. Binder, S. Tardu, P. Vezin, Cyclic modulation of Reynolds stresses and length scales in pulsed turbulent channel flow, Proc. Roy. Soc. Lond. A 451 (1995) 121–142.